BOND CHARACTERISTICS OF REINFORCING BARS
FOR SEISMIC LOADINGS

Neil M. Hawkins and I.J. Lin

SYNOPSIS

Experimental results are presented illustrating the effects of
loading history, bar size, concrete strength, end anchorage, joint hoop
reinforcement, and bar surface geometry on the load-slip characteristics
of reinforcing bars subjected to large displacements that stress those
bars inelastically. The significance of the test results for evalua-
tion of development length requirements for seismic-type loadings is
examined and a simple mathematical model for predicting load-slip
effects is reported.

RESUME

Des résultats expérimentaux sont présentés qui illustrent les
effets du mode de chargement, de la dimension de la barre, de la
résistance du béton, de l'ancrage, de l'armature en spirale des
joints et de la géométrie des barres sur les caractéristiques charge-
déplacement des armatures d'acier soumises à de grands déplacements
qui déforment les barres inélastiquement. L'importance de ces
résultats pour l'évaluation des longueurs d'ancrage des barres dans
les cas de chargement sismique est étudiée et un modèle mathématique
simple prédisant les effets charge-déplacement est présenté.

1226

Neil M. Hawkins is Professor and Chairman, Department of Civil
Engineering, University of Washington, Seattle, Washington. He
obtained his Ph.D. degree from the University of Illinois in 1961 and
has been active in earthquake engineering research since 1972.

Ing Jaung Lin is a Ph.D. Candidate in the Department of Civil
Engineering, University of Washington. He obtained his B.S.C.E. degree
from the National Taiwan University, Taipei, in 1971 and his M.S.C.E.
degree from the University of Washington in 1975.

INTRODUCTION

The bond characteristics of the reinforcing bars used in concrete
structures in seismic zones are important for two reasons. First,
slip between bars and surrounding concrete markedly affects the stiff-
ness characteristics of joints and therefore the overall response of
concrete structures to earthquakes. That slip influences both the
magnitude of the maximum forces acting on a structure and the result-
ant drifts. Second, during severe earthquakes, bars embedded in
highly stressed and cracked concrete are subjected to large inelastic
stress reversals. For such conditions, the anchorage characteristics
of bars must still be adequate to prevent pull-out type failures.

Over the past six years, tests have been conducted at the Univer-
sity of Washington on a variety of specimens simulating embedment
conditions for beam bars extending into beam-column connections. These
beam bars have been subjected to reversing forces that have stressed
them inelastically both in tension and compression. This paper summar-
izes the principal findings from these tests.

TEST SPECIMENS

In the first phase of this study, tests were made on 23 specimens
having the proportions shown in Figure 1 (1). Column moments were
simulated by single compressive restraints acting on the top and bottom
surfaces of the test specimen. In Figure 1 those restraints were R_1
and R_2 for tensile loadings, and R_1' and R_2' for compressive loadings
on the beam bar. The effects of a moment applied to the connection by
a beam were simulated by pulling or pushing on the beam bar through a
cadweld splice and reacting that force by compressive restraints, R_3
for tensile loadings and R_4 for compressive loadings on the beam bar.
The supplementary reinforcement used in the cyclic loading tests is
shown in Figure 1. Quantities were chosen so that a loaded, deformed,
No. 10 grade 40 beam bar could be stressed well into its yield range
before failure occurred. In a series of monotonic loading tests, the
amount and distribution of the No. 4 bars used as hoop reinforcement
were varied. It was shown that the hoop reinforcement indicated in
Figure 1, although poorly distributed, was more than double that
required to prevent variations in the load-displacement relationship
caused by the opening of diagonal tension cracks within the joint core.

Variables examined in the cyclic tests were the loading history for the bar; the surface geometry for the bar; and the effect of terminating the bar with a standard 180 degree hook. The loading histories compared were monotonic tensile loading to failure, cyclic loading from zero to a maximum tensile partially reversed cyclic (maximum compressive load significantly less than maximum tensile load), and fully reversed cyclic loading (maximum displacement for compressive loading equal to that for tensile loading). The effects of fully reversed cyclic loading were compared for plain bars, and bars with bamboo or alternating V-type deformations. In Figure 1 the geometry for a straight bar in the test specimen is indicated by solid lines and the geometry for a bent bar by broken lines.

In the second phase of the study, tests were made on 16 specimens having the proportions shown in Figure 2 (2, 3, 4). The test set-up and loading arrangements were similar to those for the specimens in the first phase of the study. However, in order to better simulate restraint effects provided by columns in a prototype connection, the vertical dimension of the specimen was increased considerably over that for the first phase studies, more supplementary reinforcement was provided and the depth of the simulated connection was increased. Except for one monotonic tensile test, all specimens were reversed cyclically loaded. Variables were the loading history; the use of a straight bar or a bar terminating with a standard 90-degree hook; the yield strength for the bar, grade 40 or grade 60; additional confining reinforcement in the joint; and the strength of the concrete. Most of the specimens had hoop reinforcement as indicated by the solid lines in Figure 2. Three specimens had additional hoop reinforcement as indicated by the broken lines in Figure 2. Concrete strengths were varied between 2600 and 5100 psi. No. 10 beam bars with bamboo-type deformations were used for all specimens.

In the third phase of this study, tests were made on 9 specimens having the proportions shown in Figure 3 (5). The test set-up, loading arrangements and type of specimen were similar to those for the specimens used in the second phase of the study. However, because the tests were conducted using a No. 6 bar, the width of the specimen was reduced to 16 in. and the effective depth of the simulated joint was reduced to 9 in. Grade 60 straight bars were used in all specimens. Variables were the loading history and the surface geometry for the bar. Bars with both bamboo and alternating V-type deformations were tested.

For all specimens, measurements were made of the force on the bar and the relative displacements between the point X at the "attack" end of the bar, Figure 1, and a point Y about mid-way along the length of the specimen. Relative displacements between the bar and the immediately adjacent concrete were also measured for the "tail" end of specimens with straight bars. Strains along the length of most of the bars were measured with electrical resistance gages positioned inside a groove machined in the surface of the bar. In tests conducted at the University of California at Berkeley, it has been shown that good correspondence can be established between experimental results for grooved and ungrooved bars if loads are related on the basis of the effective lug perimeter (6). Comprehensive details concerning material

properties and the test procedures are given in References (1), (2), (4) and (5). All specimens were proportioned so that the loaded deformed bars yielded at displacements considerably less than those for failure. Except for the specimens with No. 10, grade 60 straight bars, development lengths were equal to or greater than the lengths required according to ACI 318-77.

TEST RESULTS

Typical relationships between the axial force on a bar and the relative displacement at the "attack" end are shown in Figures 4 through 16. The broken lines on each load-displacement diagram represent the result for a specimen identical to that shown, having a straight bar and loaded monotonically to failure. The concrete strengths for the monotonically loaded specimens were 3,000 psi, 2890 psi and 2900 psi for specimens from References (1), (2), (4) and (5), respectively. Also shown on each figure are load histories defined in terms of ductility ratios for successive half cycles. The ductility ratio was taken as the relative displacement at the attack end between the displacement for the previous zero load and the displacement for the maximum load divided by the relative displacement for yielding in the first inelastic half cycle. The displacements for first yielding were very similar for all specimens and equal to 40×10^{-3} inches. Cylinder compressive strengths for each specimen are shown on each figure.

When comparisons were made between results for connections identical except for the form of the specimen, Figure 1 or Figure 2, the form was found to have little effect on the load-displacement relationship. Shown in Figure 4 is a typical relationship for a specimen showing little bond deterioration. For increasing displacements, hysteresis loops remained wide and had shapes reflecting the stress-strain properties for the bar. Further, when cycling was discontinued and the specimen loaded to failure in tension, the maximum load that was achieved and the corresponding displacement were similar to those for a specimen loaded monotonically to failure. Shown in Figure 5 is a typical relationship for a specimen containing a straight bar showing bond deterioration and finally undergoing a pull-out failure. The hysteresis loops had forms similar to those shown in Figure 4 until the second cycle to a ductility ratio of three. With further cycling and with increasing displacements, the loops then became distinctly S-shaped. The capacity at the peak slip decreased and the concrete cover over the column steel at both the "attack" and "tail" ends of the bar spalled off.

From comparisons and analyses of test results such as those shown in Figures 5 through 14, it has been established that:

(1) The characteristics of the loading history have a marked effect on the rate of bond deterioration and the mode of failure. The rate of bond deterioration increased as the ratio of the peak compressive to peak tensile load increased. Two modes of failure have been observed:

    (a) Collapse following attainment of the same ultimate load and

deformation capacities as those obtained for a similar specimen loaded monotonically to failure, and

(b) collapse due to bond deterioration at an ultimate load considerably less and at an ultimate deformation as little as one-third of that for a similar specimen loaded monotonically to failure. Collapse in the latter mode generally occurred when the bar was reversed cyclically loaded to yielding both in tension and compression. If, however, reversed cyclic loading was discontinued before failure and the specimen then loaded monotonically to failure, the failure mode reverted to type (a). Shown in Figure 6 is the load-displacement curve obtained with a No. 10, grade 40 straight bar subjected to cyclic tensile loadings. The behavior was almost identical to that for monotonic loading and there was little change in stiffness with cycling. Shown in Figure 7 is the load-displacement curve for a similar specimen subjected to fully reversed ductility ratios. The stiffness degenerated continuously with cycling. Failure effectively occurred at the maximum compressive ratio for the fourth cycle although slip along the entire length of the bar was not obtained until the tensile portion of the sixth cycle.

(2) The surface geometry for the bar had a significant effect on the rate of bond deterioration. The rate increased as the ratio of the lug spacing to bar diameter increased. Bars with different surface geometries and similar load-displacement characteristics for monotonic loading had significantly different characteristics for reversed cyclic loading. The load-displacement curve shown in Figure 7 is for a No. 10, grade 40 straight bar with bamboo-type deformations. The curve shown in Figure 8 is for a similar bar with V-type deformations. It is obvious that while the stiffness degeneration characteristics with cycling for the two specimens were similar, the bar with V-type deformations had superior ductility. The result was similar for comparisons of bars terminating with 90 and 180-degree standard hooks and for No. 6 straight bars. Typically for cycling between the constant peak displacements, the number of cycles for failure for V-type lugs was about double that for bamboo-type lugs.

(3) For reversed cyclically loaded hooked bars, bond resistance and energy absorption were provided initially by the "lead-in" length to the hook and there was a change in behavior once slip penetrated to the end of that "lead-in" length. Shown in Figure 9 is the load-displacement curve for a bar terminated with an 180-degree hook. Except for the hook, the properties of the specimen shown in Figure 9 were the same as those of the specimen shown in Figure 8. The response for specimens with 180-degree hooks was much poorer than that for specimens with straight bars because once slip penetrated to the hook, the motions of the hook broke up the connection. Shown in Figure 10 is the load-displacement curve for a specimen with a No. 10, grade 60 straight bar, and shown in Figure 11 is the curve for the same bar terminated with a 90-degree hook. The 90-degree connection maintains good characteristics for tensile loading considerably longer than for compressive loading but even then its characteristics are not nearly as good as those for the specimen with a straight bar. An additional advantage for a 90-degree hook over an 180-degree hook is that for tensile loadings to displacements greater

than the displacement for the peak capacity, there is some regain of strength with increasing tensile displacements. However, that gain is lost rapidly with cycling. Further, for compression loadings, there was no gain and the bars behaved as if they were straight. The appearance of test specimens with hooks after failure suggests that in buildings surviving an earthquake, loss of cover from behind the hook should be taken as indicating that anchorage for such bars has been destroyed.

(4) The grade of the bar had less effect than the general form of its stress-strain characteristics. The slope of the load-displacement curve after yielding depends on the length of the yield plateau in the bar's stress-strain curve and the bar's strain hardening modulus. For bars with similar strain hardening moduli, the slope of the post-yield load-slip curve decreased as the length of the yield plateau increased and for bars with similar yield plateau lengths, the slope of the post-yield load-slip curve increased as the strain-hardening modulus increased. Thus, the total response was an averaging of two effects. That behavior reflects the manner in which stresses built up along the bar. Strain measurements showed that anchorage lengths of only 10 bar diameters were needed to develop yielding in a grade 60 bar and about 8 bar diameters for a grade 40 bar. When a bar is first stressed inelastically, any yielding length is small and the initial slope of the post-yield load-slip curve depends primarily on the strain-hardening modulus. However, the bond stress that can be developed with a yielding bar is considerably less than that with an elastic bar. Therefore, for increasing loads beyond yielding, the length of bar that is yielding increases rapidly and the length of the yield plateau becomes increasingly important in determining the slope of the load-slip curve. Comparison of the curves for Figures 7 and 10 shows the effects of bar grade on response. The displacement at the maximum load was approximately inversely proportional to the yield strength of the bar.

(5) The strength of the concrete had a marked effect on the load-displacement curves. The displacement corresponding to the maximum load capacity increased in direct proportion to the concrete compressive strength. Comparison of the curves for Figures 12, 13 and 14 shows the dramatic effect of increasing the concrete strength from 3000 psi through 4100 psi to 5120 psi. All specimens contained No. 10, grade 60 straight bars. The comparison curve for monotonic loading is for a specimen with a concrete strength of 2890 psi. It is apparent that with a doubling of the concrete strength, the effects of fully reversed cyclic loading can be largely offset.

(6) Additional hoop reinforcement, placed as described previously in the discussion of Figure 2, markedly improved the load-displacement characteristics for bars terminating with 90-degree hooks but had little effect on the characteristics for straight bars. Shown in Figure 15 is the load-displacement curve for a connection containing additional hoop steel and a bar terminating in a 90-degree hook. Shown in Figure 16 is the curve for a similar connection without additional steel and having a 1000 psi higher concrete compressive strength than the specimen shown in Figure 15. The effect of additional hoop steel was greater than the effect of the higher concrete compressive strength.

The cyclically loaded, straight bar specimen shown in Figure 12 contained additional hoop steel. Comparison of the characteristics for that specimen with those for the specimens of Figures 13 and 14 with higher concrete strengths and without additional hoop steel, demonstrates that added steel had little effect for specimens with straight bars.

SIGNIFICANCE OF RESULTS

The assumption that the joints of reinforced concrete structures can be taken as rigid for purposes of seismic analysis is incorrect. Reinforcing bars pull-out causing rigid body rotations at the connections between flexural members and columns.

A mathematical model capable of predicting the load-displacement curves measured in the first phase of this investigation was reported in Reference 7. Shown in Figure 17 is a comparison between the measured moment-rotation responses of beam-column subassemblages II and V tested by the Portland Cement Association (8) and the responses predicted by that model when all the rotation of the beam with respect to the column was assumed to be caused by slip of the reinforcement within the joint. The moment-rotation relationships are those for the first major inelastic cycle applied to the specimens. Subassemblage II had hoop reinforcement in the joint more than adequate to prevent any marked effect on the specimen's response of diagonal cracking or bulging within the joint core. Except for a complete absence of joint reinforcement, specimen V was identical to specimen II. For specimen II, the theoretical and measured moment-rotation relationships are in close agreement. For specimen V the agreement is much poorer. That result is to be expected since the load-slip data used was that for specimens with "adequate" hoop reinforcement and the post-yield load-slip characteristics deteriorate rapidly as the hoop reinforcement is reduced below the "adequate" level. While the model of Reference 7 can be used to predict failure conditions, it also has several major drawbacks. That model cannot be readily used in design because the length of embedment must be known in order to apply it. The model cannot be readily applied to a bar continuous through a joint. The length of a joint directly affects predictions even for applied loads well below those for failure. The model utilizes a maximum bond stress that is derived as a function of the external loading. Tests (9) on short lengths of bars bonded in the central portion of concrete blocks have shown that some of the extremely high maximum bond stresses predicted by that model cannot be developed. The responses predicted by that model were in reasonable agreement with the results obtained in the second and third phases of this study provided the connection contained bar sizes, concrete strengths and steel yields within about 20 percent of those used in the specimens of the first phase. Predictions were considerably poorer for specimens with properties outside that range.

In Reference 10 it is shown that the simplified mathematical model of Figure 18 can be used to determine reasonable values for bond-slip effects for slab-to-column connections transferring reversing moments. The curve OABC defines the response for monotonic tensile loading and OB'C' the response for monotonic compressive loading. The slip at

yielding, S_Y, equals the yield force for the bar P_Y, times the bond-slip stiffness, K. The value of K, in kips per inch, is calculated from the following equation:

$$K = (1,250\ D^2 + 1,900)\ (\sqrt{\frac{f_c'}{3200}}) \qquad (1)$$

where D is the bar diameter in inches. Equation (1) is applicable for D values ranging from 0.5 through 2.25 inches. In Figure 18 the proposed cyclic load model is indicated by thick unbroken lines. Typical test results are indicated by broken lines. Rules for construction of the model are as follows:

Condition 1--The yield load P_Y has not been exceeded. The bar force is P_1. Unloading follows a straight line from A towards E. The unloading stiffness, K, is twice that given by Equation (1). Once the direction of loading reverses, the stiffness reverts to K. When unloading commences at A', the stiffness again changes to 2K.

Condition 2--The yield load, P_Y, has been exceeded for tensile loading. The bar force is P_Y and the slip S_2. The capacity decreases with no change in slip until the initial yield load is reached. The unloading stiffness then becomes 2K until the load drops to zero. For compressive loadings, the response follows a straight line directed towards the load and slip for yielding in compression B'. When unloading commences at the slip, S_2', the stiffness is 2K until the load drops to zero. For tensile loadings, the response then follows a straight line directed towards the load and slip for yielding in tension.

The tests reported here and in References (6) and (11) show that ACI Code 318-77 provisions for embedment length are inapplicable to reversed cyclic loadings. Those provisions are designed to insure a bar's yield under monotonic loadings. For adequate seismic resistance, provisions should ensure that for reversed cyclic loadings, bar strengths greater than the yield strength can be developed for attack end displacements up to ten times greater than those for first yielding. None of the test results shown in Figures 4 through 16 satisfy those criteria. The only test specimen reported in References (1, 2, 4 and 5) that satisfied these criteria had theoretically an equivalent embedment length of 37.7 inches compared to a basic development length required according to ACI 318-77 of 23.0 inches for the nominal grade of the bar and 27.0 inches based on the actual yield strength of the bar. The formulas recommended by ACI-ASCE Committee 352 (12) result in more realistic requirements for development length provided additional length is added to recognize that the concrete beyond the line of the column reinforcement at the loaded end of the bar is ineffective for anchorage.

CONCLUSIONS

Based on the results reported here, the following conclusions are warranted:

1. The joints between flexural members and columns should not be assumed to be rigid for seismic-type loadings. The load-slip characteristics for bars are as important as their stress-strain characteristics for predictions of the response of plastic hinge regions in seismically loaded structures.

2. The load-slip model shown in Figure 18 can be used to predict reasonable values for slip effects. The concentrated rotations caused by bond slip of the slab bars within a slab-column joint typically doubles the inter-story drifts predicted at first yield of those bars.

3. The formulas recommended in Chapter 12 of ACI Code 318-77 for basic development length are inapplicable to inelastic, reversed cyclically loaded bars.

1234

REFERENCES

(1) Hassan, F.M., and Hawkins, N.M., "Anchorage of Reinforcing Bars for Seismic Forces," Reinforced Concrete in Earthquake Zones, SP-53, American Concrete Institute, Detroit, 1977.

(2) Hawkins, N.M., Kobayashi, A.S., and Fourney, M.E., "Reversed Cyclic Loading Bond Deterioration Tests," Report SM 75-5, Department of Civil Engineering, University of Washington, Seattle, November 1975.

(3) Hawkins, N.M., Kobayashi, A.S., and Fourney, M.E., "Use of Acoustic Emission and Holographic Techniques to Detect Debonding in Cyclically-Loaded Concrete Structures," Proceedings of ASCE-EMD Specialty Conference, University of California, Los Angeles, March 1976.

(4) Lin, I.J., "Anchorage Characteristics of Reinforcing Bars Subjected to Reversed Cyclic Loading," Department of Civil Engineering, University of Washington, January 1978.

(5) Aminian, K., "Effect of Cyclic Loading on Bond Deterioration of No. 6 Reinforcing Bars," M.S.C.E. Thesis, University of Washington, June 1977.

(6) Popov, E.P., Bertero, V.V., and Viwathanatepa S., "Bond in Interior Joints of Ductile Moment-Resisting R/C Frames, Part I: Experiment," Presented at ACI Fall Convention, Houston, Texas, November 1978.

(7) Hassan, F.M., and Hawkins, N.M., "Prediction of Seismic Loading Anchorage Characteristics of Reinforcing Bars," Reinforced Concrete in Earthquake Zones, SP-53, American Concrete Institute, Detroit, 1977.

(8) Hanson, N.W., and Conner, H.W., "Seismic Resistance of Reinforced Concrete Beam-Column Joints," Structural Division Journal, ASCE, October 1967.

(9) Liu, Y.H., "Local Bond Strength of Concrete Under Cyclic Loading," M.S.C.E. Thesis, University of Washington, 1978.

(10) Hawkins, N.M., Wong, C.F., and Yang, C.H., "Slab-Edge Column Connections Transferring High Intensity Reversing Moments Normal to the Edge of the Slab," Report SM 78-1, Department of Civil Engineering, University of Washington, May 1978.

(11) Popov, E.P., Bertero, V.V., Cowell, A.D., and Viwathanatepa S., "Reinforcing Steel Bond Under Monotonic and Cyclic Loading," SEAOC Conference, Lake Tahoe, September 1978.

(12) ACI-ASCE Committee 352, "Recommendations for Design of Beam-Column Joints in Monolithic Reinforced Concrete Structures," ACI Journal, Vol. 73, No. 7, July 1976.
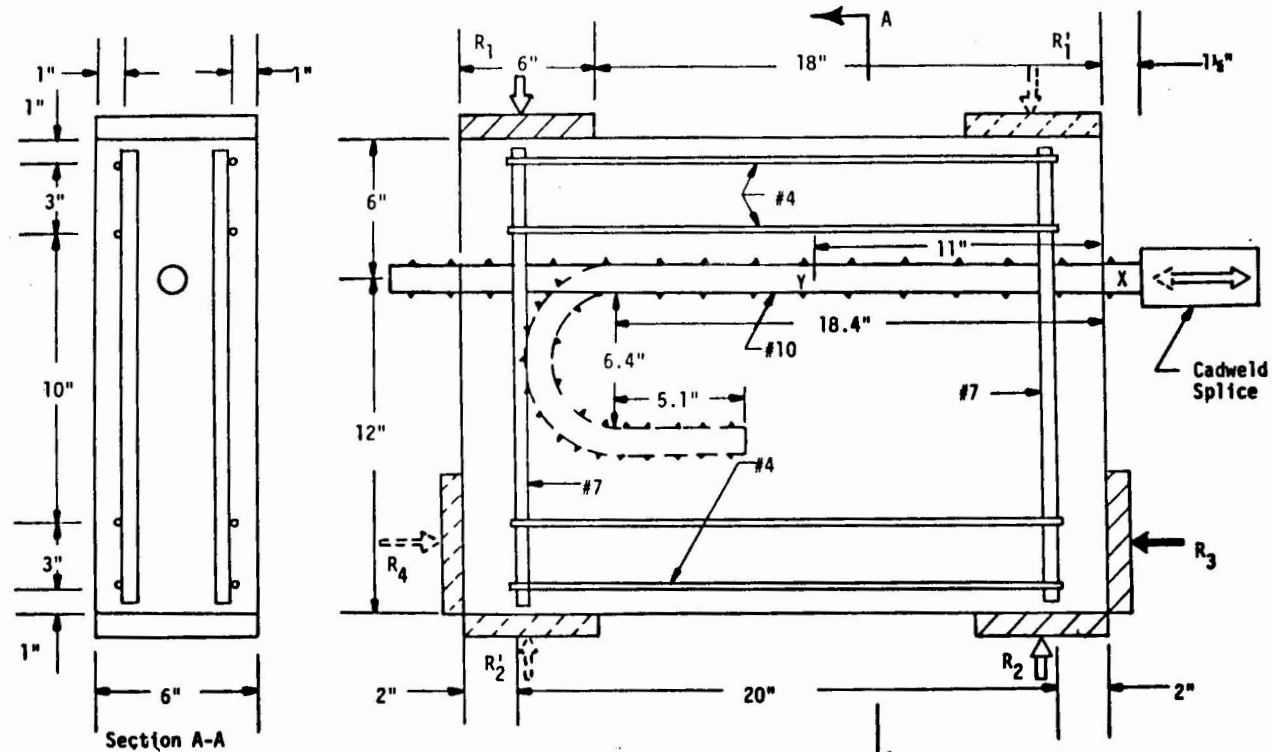
- All Reinforcing Bars are Grade 40
- Shaded Areas are Supports

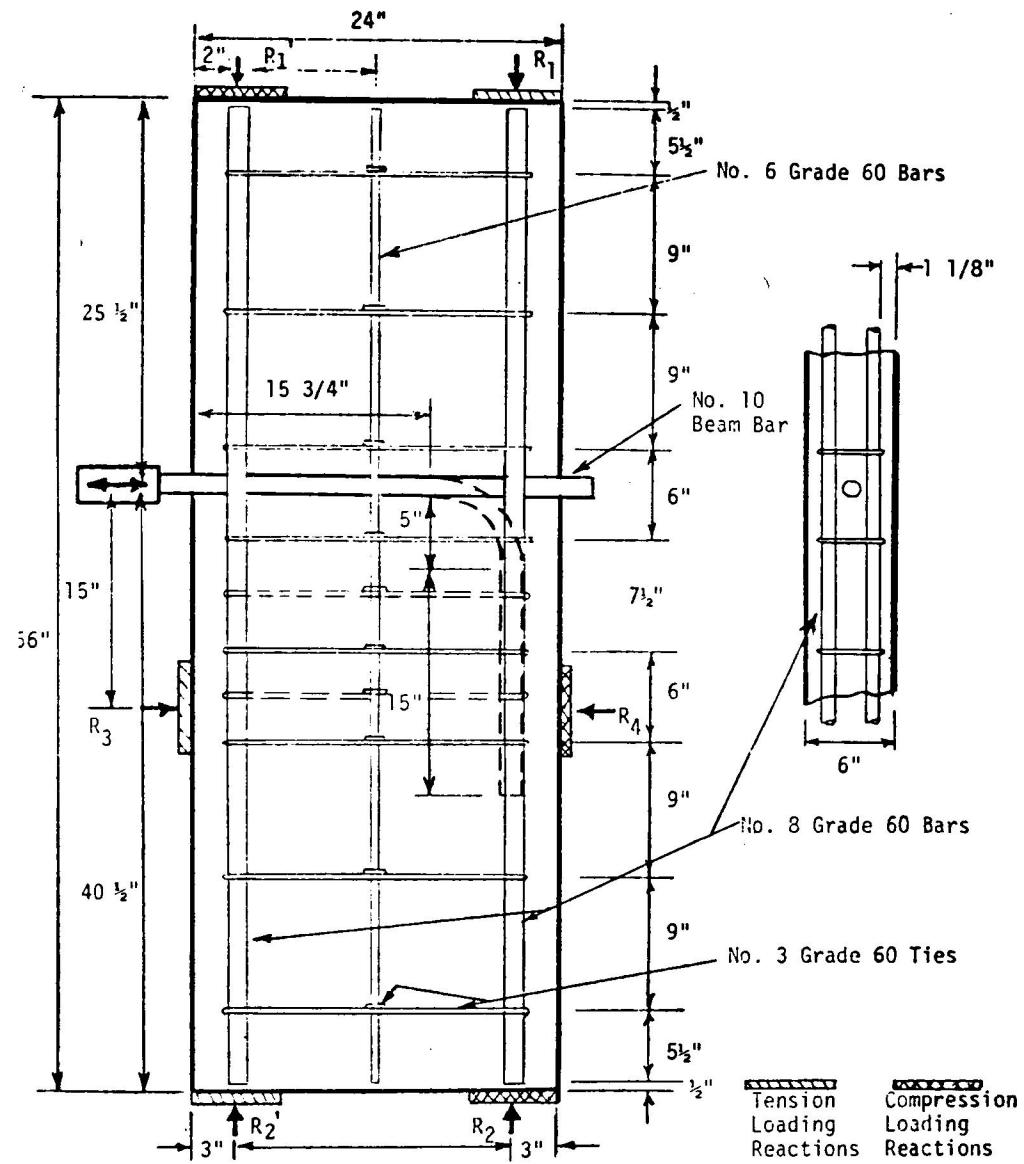Figure 1   Test specimens--Reference (1).

1236

Figure 2   Test specimens--References (2, 3 and 4).
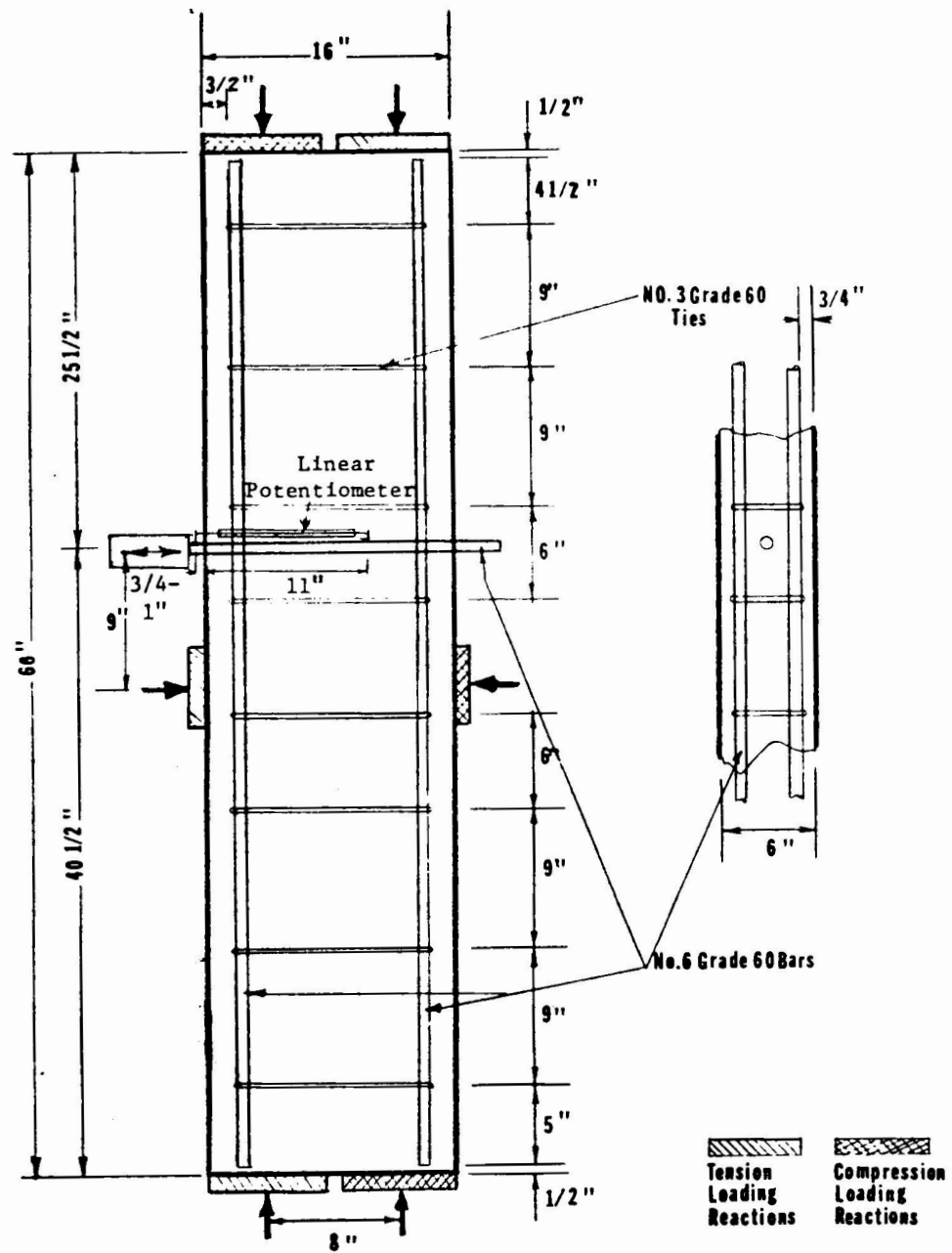
Figure 3   Test specimens--Reference (4).
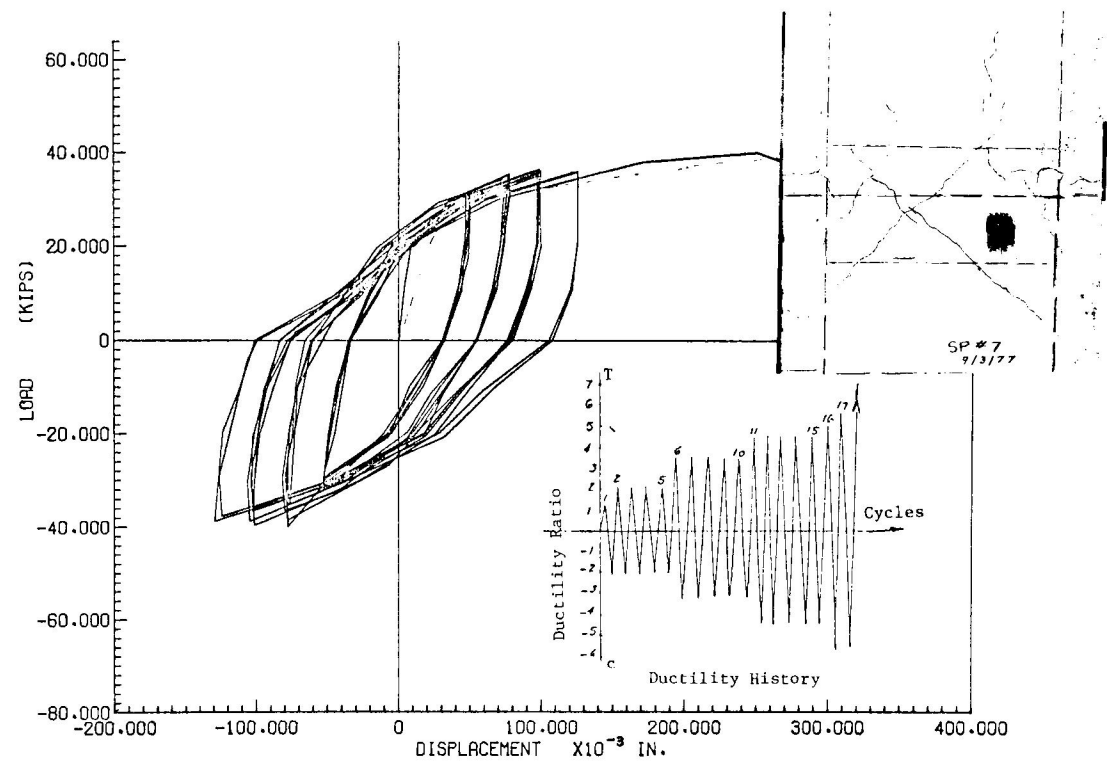
Figure 4   Load-displacement curve, specimen K7, Reference (4),
            No. 6 straight bar, bamboo-type deformations,
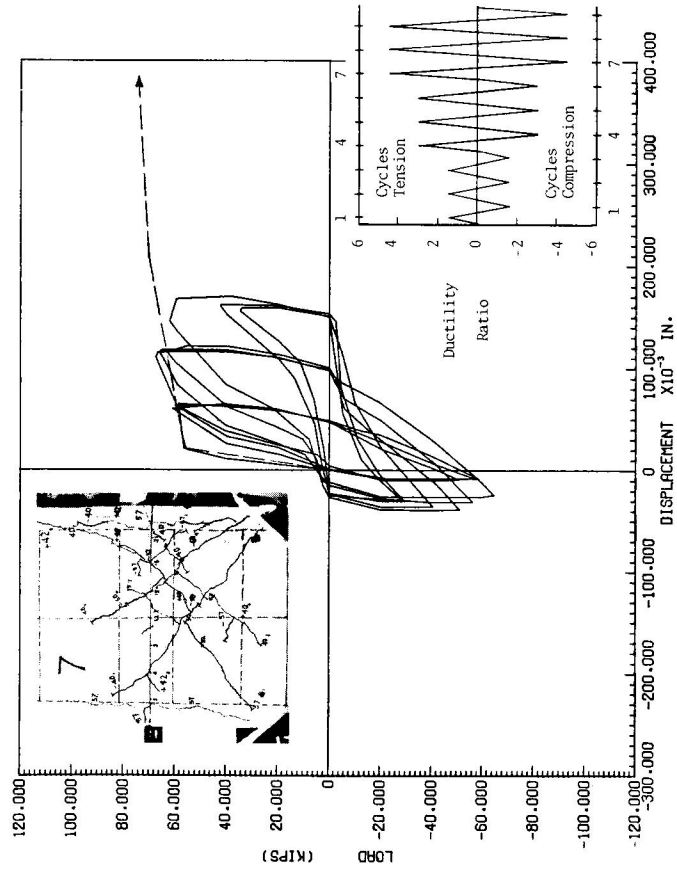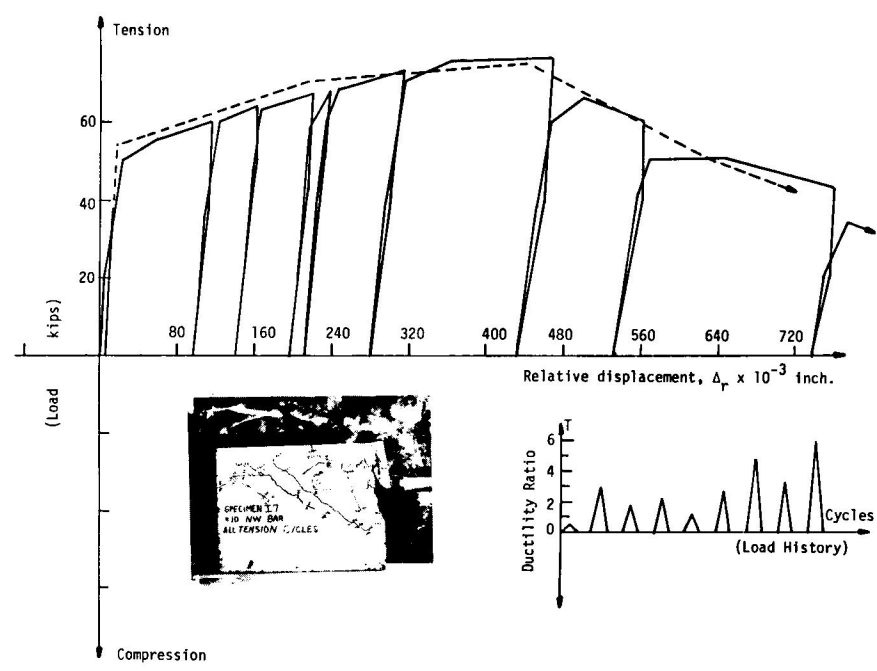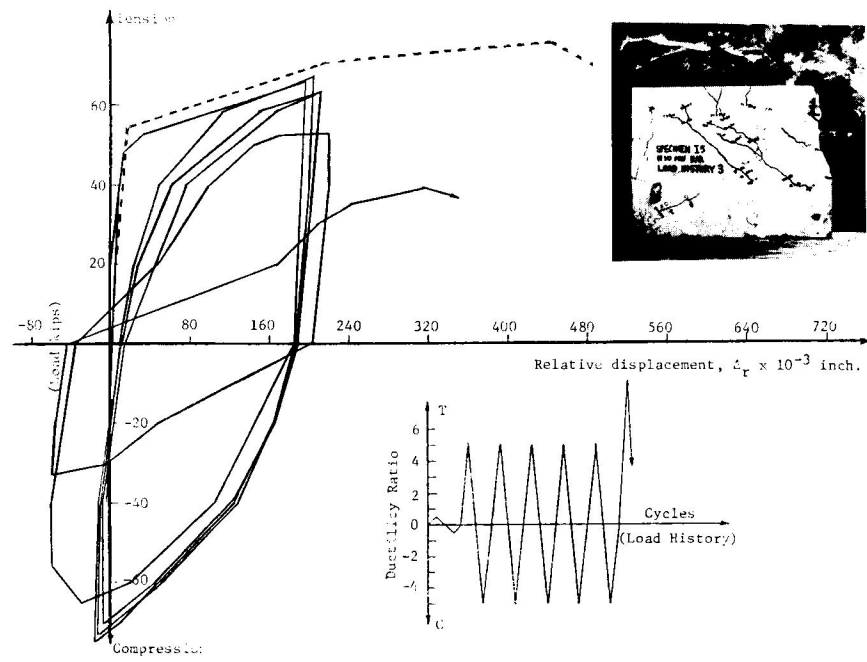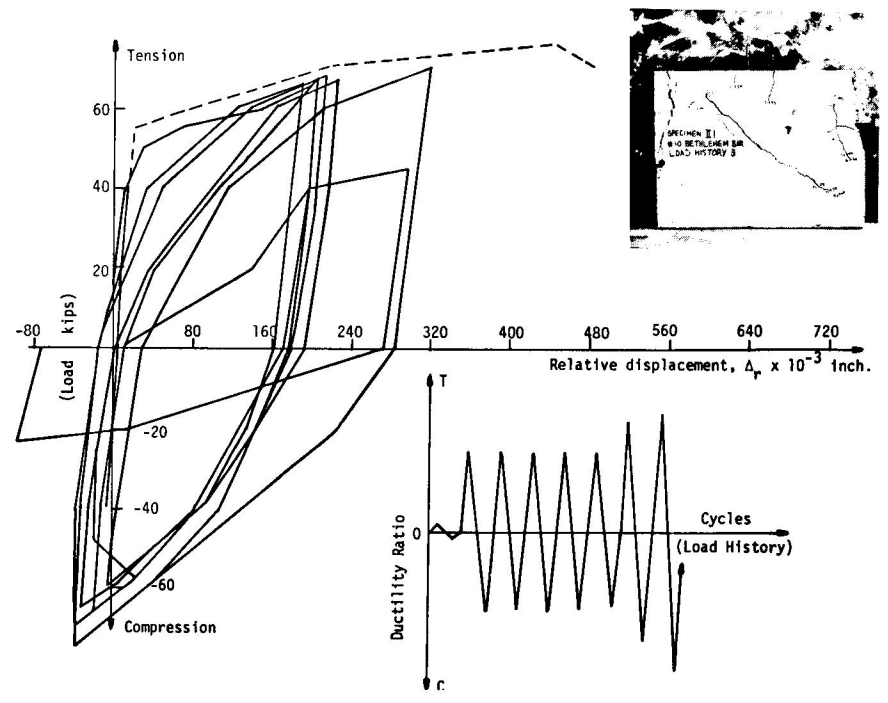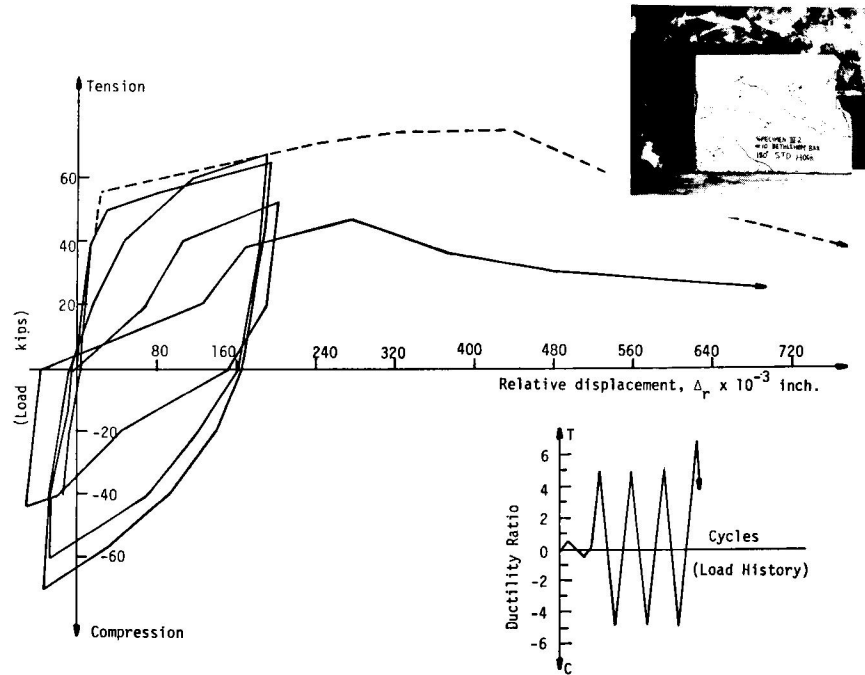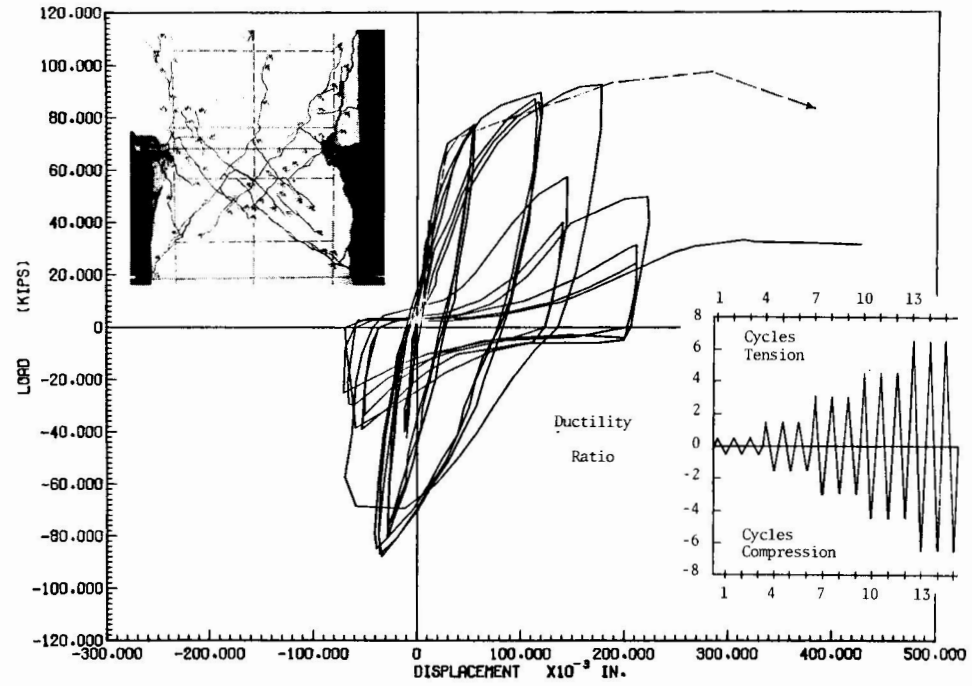 f_Y = 67 ksi, $f_c{}'$ = 3,400 psi.

Figure 5   Load-displacement curve, specimen L7, Reference (2),
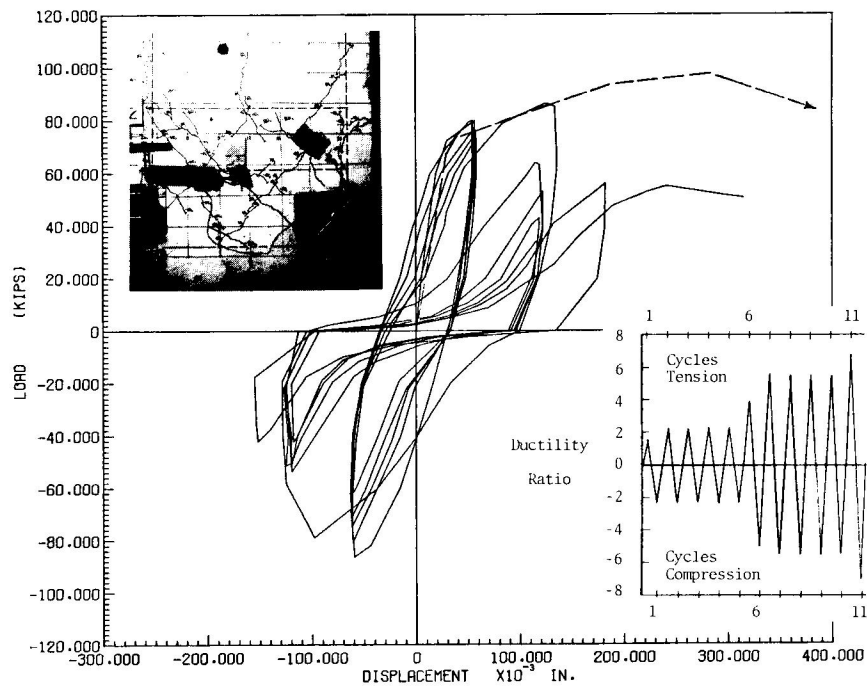No. 10 straight bar, bamboo-type deformations,
f_Y = 48 ksi, f_C' = 2,640 psi.

Figure 6   Load-displacement curve, specimen 6, Reference (1),
No. 10 straight bar, bamboo-type deformations,
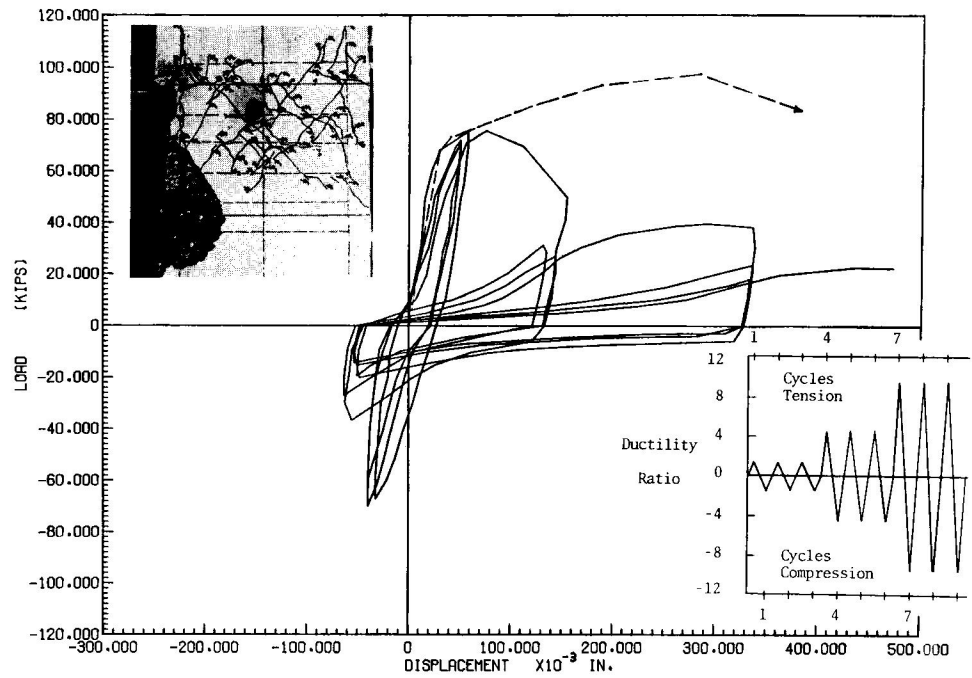f_Y = 48 ksi, f_c' = 3,100 psi.

Figure 7   Load-displacement curve, specimen 4, Reference (1),
            No. 10 straight bar, bamboo-type deformations,
            f_Y = 48 ksi, f_c' = 4,200 psi.

Figure 8   Load-displacement curve, specimen 8, Reference (1),
No. 10 straight bar, V-type deformations,
f_Y = 48 ksi, f_c' = 3,300 psi.

Figure 9   Load-displacement curve, specimen 13, Reference (1),
No. 10 bar, 180-degree hook, V-type deformations,
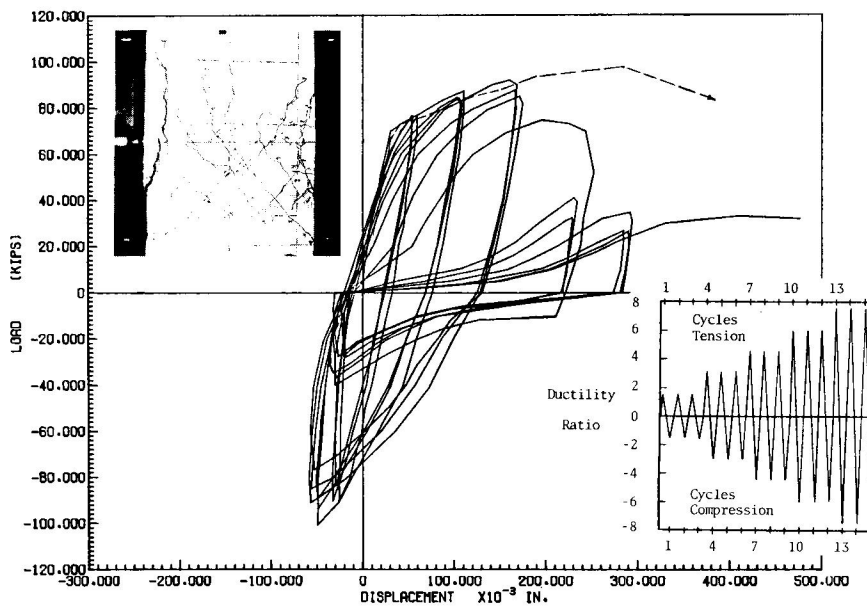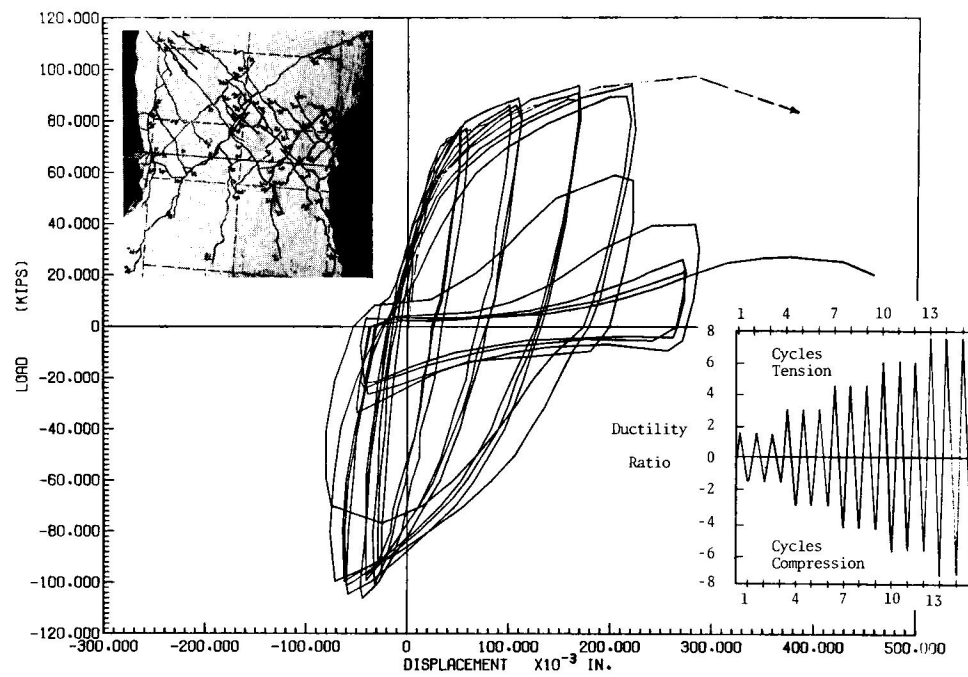f_Y = 48 ksi, f_C' = 3,100 psi.

Figure 10   Load-displacement curve, specimen L16, Reference (4),
No. 10 straight bar, bamboo-type deformations,
f_Y = 60 ksi, f_c' = 3,760 psi.

Figure 11   Load-displacement curve, specimen L9, Reference (2),
No. 10 bar, 90-degree hook, bamboo-type deformations,
f_Y = 60 ksi, f_C' = 3,050 psi.

Figure 12   Load-displacement curve, specimen L14, Reference (4),
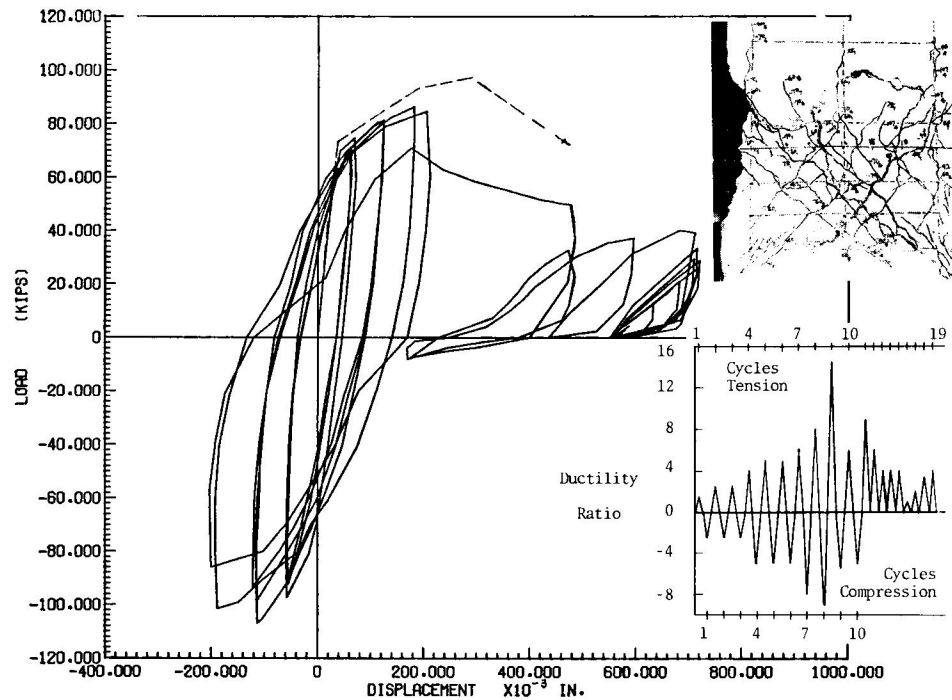No. 10 straight bar, bamboo-type deformations,
f_y = 60 ksi, f_c' = 3,000 psi, additional hoop steel.

Figure 13   Load-displacement curve, specimen L13, Reference (4),
No. 10 straight bar, bamboo-type deformations,
f_y = 60 ksi, f_c' = 4,100 psi.

Figure 14   Load-displacement curve, specimen L15, Reference (4),
No. 10 straight bar, bamboo-type deformations,
f_y = 60 ksi, f_c' 5,120 psi.

Figure 15   Load-displacement curve, specimen L12, Reference (4),
            No. 10 bar, 90-degree hook, bamboo-type deformations,
            f_y = 60 ksi, f_c' = 4,110 psi, additional hoop steel.
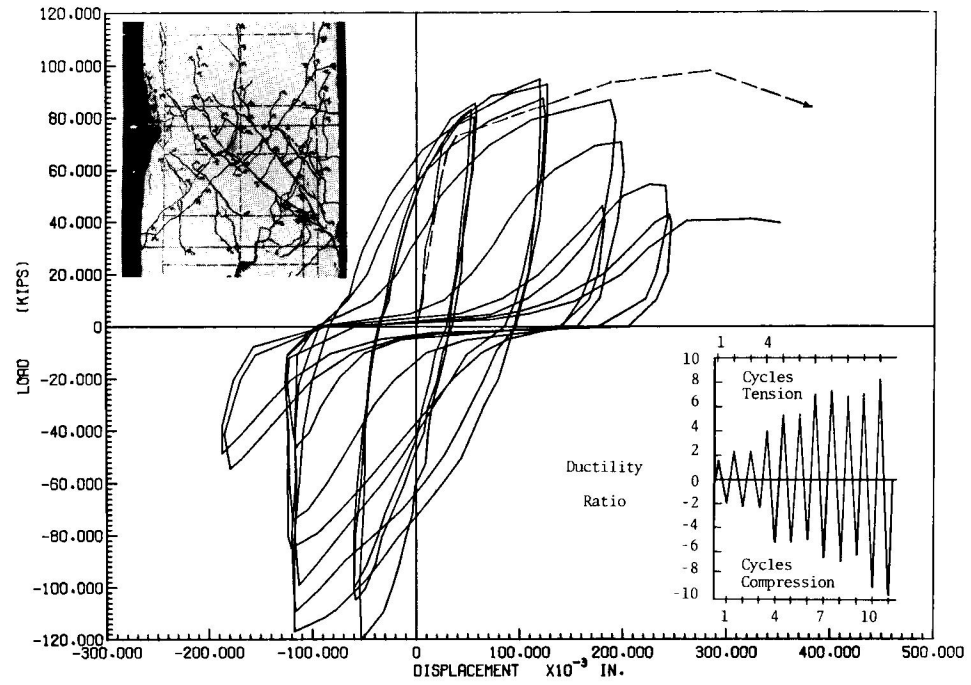
Figure 16　Load-displacement curve, specimen L17, Reference (4), No. 10 bar, 90-degree hook, bamboo-type deformations, f_Y = 60 ksi, f_c' = 5,060 psi.
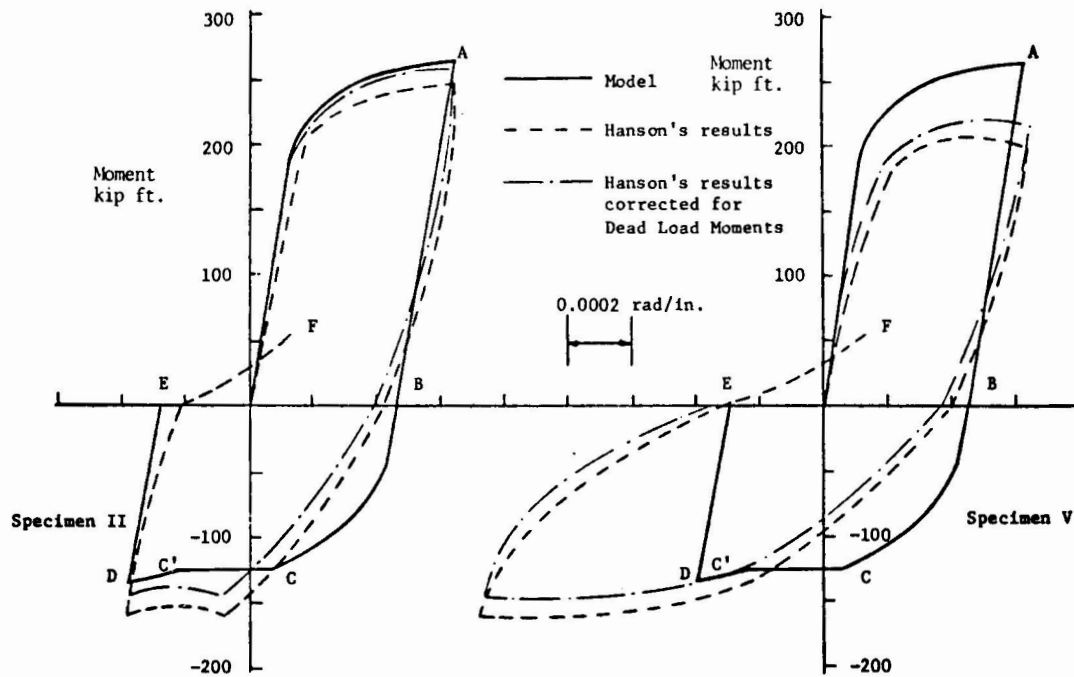
Figure 17   Comparison of predictions of model of Reference (7) with
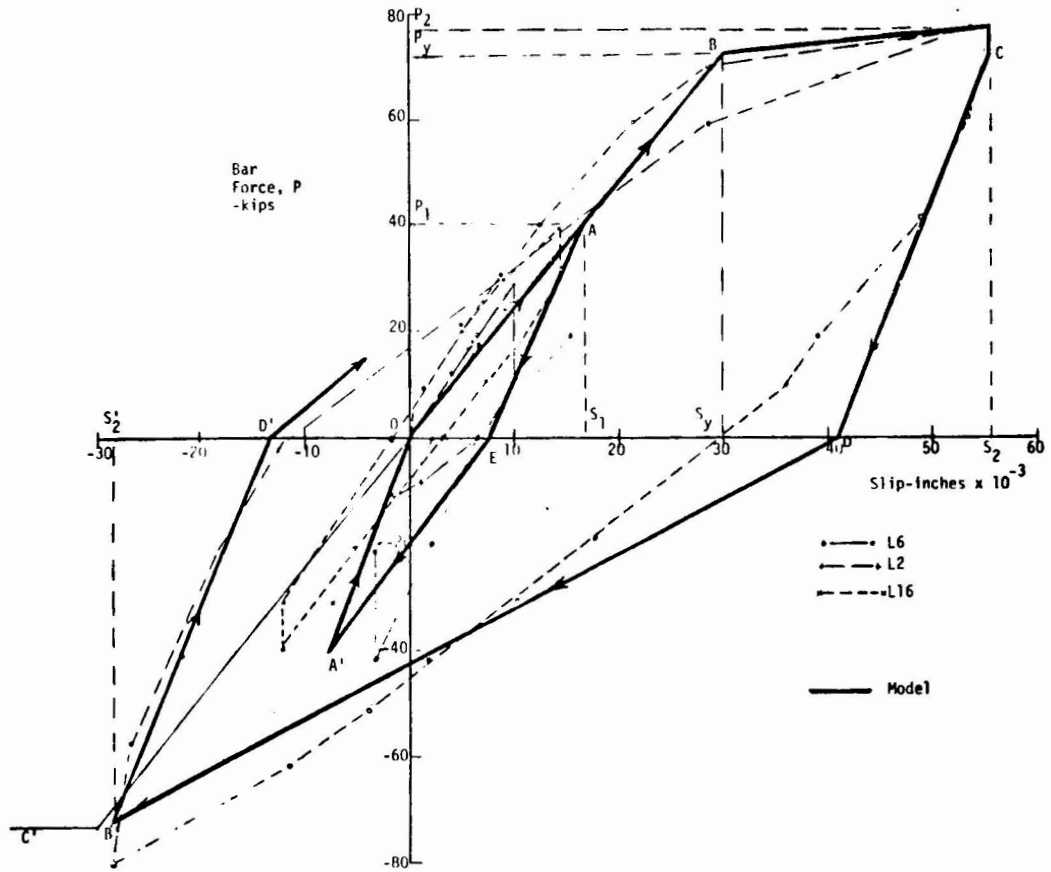beam-column results of Reference (8).

Figure 18   Bar force-pull out model for cyclic loading.